Supplementary Information

Promotion of Electrochemical Reduction of CO_2 over Cu_2O-Cu (111) Interface Assisted by Oxygen Vacancies

Shuang Xu[#], Lei Yang[#], Congya Wang, Liwei Pan, Jing Zhang, Yaling Wang， Hexiang Zhong*

Supplementary Note 1. Faraday efficiency calculation for ECR

In this chapter, Faraday efficiency (FE) serves as a critical metric for assessing the product selectivity in the electrocatalytic reduction of CO_2 by a catalyst. Faraday efficiency refers to the percentage of electricity that is effectively utilized in converting CO_2 into a specific product, relative to the total electricity consumed throughout the reaction process.

The Faraday efficiency of the gas product is calculated as follows:

$$FE_j = \frac{nfV_j vP_0}{RT_0 I_{total}} \times 100\% \#(1)$$

Let *n* represent the number of electrons transferred from a single CO_2 molecule to a gaseous product, with n having a value of 8. The Faraday constant, denoted by *F*, is given as 96485 C mol^{-1}. The volume percentage of the gaseous product is represented by V_j. The flow rate of the gas into the gas chromatograph is denoted by *v*, measured in mL min^{-1}. The standard atmospheric pressure, P_0, is 1.01×10^5 Pa. The gas constant, *R*, is 8.314 J mol^{-1} K^{-1}. The absolute zero temperature, T_0, is 273.15 K. Lastly, I_{total} denotes the total current during the reaction, measured in mA.

The Faraday efficiency of the liquid phase product is calculated as follows：

$$\mathrm{FE} = \frac{nFCV}{\int_0^t Idt} \times 100\% \#(2)$$

Where *n* represents the number of electrons transferred from a single CO_2 molecule to a gaseous product, with a value of 2; *F* is Faraday's constant, which is 96485 C mol^{-1}; *C* is the concentration of formate ions in the electrolyte, measured in mol L^{-1}; *V* is the volume of the electrolyte, measured in L; *I* is the current intensity during the reaction, measured in amperes (A); and *t* is the reaction time, measured in s.

Supplementary Note 2. Crystal surface characterized by selected area electron diffraction (SAED) analysis

Complementary selected-area electron diffraction (SAED) analysis (**Fig. S1**) revealed characteristic ring-like diffraction patterns, which conclusively confirm the polycrystalline structure of the synthesized material. Combined with high-resolution transmission electron microscopy images, this data demonstrates the dominance of the (111) crystal plane in the bulk phase.

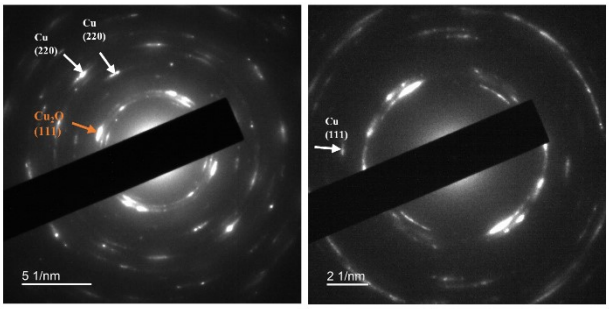

Figure S1. The selected-area electron diffraction (SAED) analysis images of OR-Cu/CM catalyst

Supplementary Note 3. Surface composition characterized by X-ray photoelectron spectroscopy

The chemical components and states of the CM, O-Cu/CM and OR-Cu/CM catalysts were further explored by XPS. Elements including O, C and Cu can be observed in the full range XPS survey of these samples.

Atomic	CM	O-Cu/CM	OR-Cu/CM
C	75.4	54.74	76.66
Cu	9.08	4.43	8.26
O	15.52	40.84	15.08

Table S1. Atomic content of C, Cu and O in CM, O-Cu/CM and OR-Cu/CM catalyst

Supplementary Note 4. Electrochemical characterization of electrocatalyst

As shown in **Table S2**, in order to assess the activity of the electrocatalysts, Electrochemical Impedance Spectroscopy (EIS) were performed on the prepared OR-Cu/CM, O-Cu/CM and CM electrodes in N_2 saturated 0.5 M KCl solution to compare the performance of the three mesh electrodes in catalyzing the CO_2 reduction. **Fig. S2. (a)-(c)** Cyclic voltammograms of copper mesh (geometrical area of 2 cm^2) in nitrogen saturated 0.1 M KCl after different treatments in the region of -0.55 V to - 0.25 V. at scanning rates from 100 to 300 mV s^{-1}. All pretreatment reactions All pretreatment reactions were carried out in 0.1 M KCl saturated with carbon dioxide. Plot as a function of scan rate. Double layer capacitance (Cdl) calculated from the slope is also shown Double layer capacitance (Cdl) calculated from the slope.

Electrodes	Rs	Rct
CM	5.016	1.914
O-Cu/CM	6.122	2.239
OR-Cu/CM	4.952	0.01202

Table S2. The Rs and Rct of CM, O-Cu/CM and OR-Cu/CM catalyst

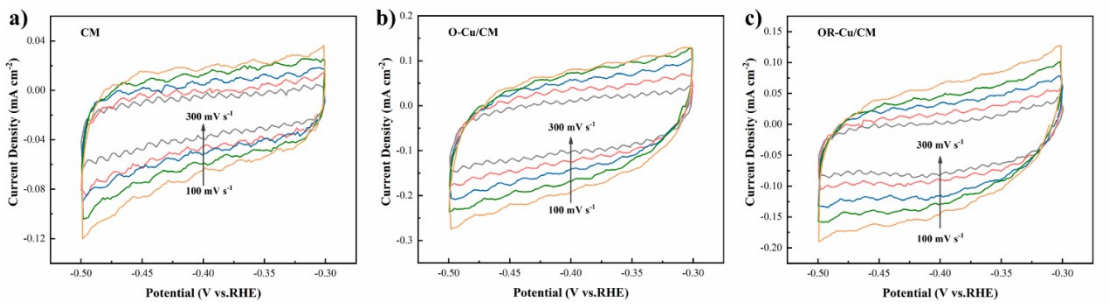

Figure S2. The cyclic voltammetry curve (CV) of CM, O-Cu/CM and OR-Cu/CM catalyst (a, b, c) in CO_2-saturated 0.5 M KCl.

Supplementary Note 5. Performance comparison and material design of current and previous copper-based catalysts

To evaluate the material design and performance superiority of the electrocatalysts, data from existing and prior copper-based catalysts were compiled for benchmarking the performance of electrocatalytic CO_2 reduction to methane (**Table S3**). A key result of this catalyst is the oxygen-deficient Cu_2O-Cu interface formed through continuous copper substrate-mediated anodic oxidation and electrochemical reduction. As indicated in **Table S3**, the OR-Cu/CM catalyst exhibits CH_4 selectivity is relatively high among the reported values. Additionally, it achieves high current density under low overpotentials.

Table S3. Performance comparison and material design of current and previous copper-based catalysts in CO_2 electroreduction to CH_4.

Catalyst	Potential (V vs. RHE)	j ($mA \cdot cm^{-2}$)	FE_{CH4} (%)	Reactor/ Electrolyte	Material Design	Ref.
Cu_2O-Cu (111)	-1.38	~41.5[b]	~56.6	H-cell 0.5 M KCl	Continuous anodic oxidation and electrochemical reduction driven by a copper substrate to create an oxygen-deficient Cu_2O-Cu interface.	This work
Cu-NC-1-4	-1.60	~41[a]	~67.2	H-cell 0.5 M $KHCO_3$	Copper single-atom catalysts (Cu-NC) supported on a carbon substrate are synthesized using a one-pot method.	[1]
m-Cu NPs	-1.30	~7.5[b]	~50	Flow-cell 1 M $KHCO_3$	Highly-dispersed copper nanoparticles (Cu NPs) were directly synthesized via electrochemical reduction of Cu-MOF-74, utilizing its one-dimensional porous architecture both as a precursor and a structural template.	[2]
Cu0.05-CN	-1.20	~7.97[b]	~49	H-cell 0.1 M $KHCO_3$	Atomic Cu sites are engineered within the nitrogen cavities of graphitic carbon nitride (g-C3N4).	[3]
CuTAPP	-1.63	~290.5[b]	~54.8	H-cell 0.5 M $KHCO_3$	The design of a copper porphyrin with donor-acceptor architecture integrates an amino group as electron-donating moiety at the molecular periphery, which synergistically coordinates with the central CuN_4 electron-accepting center.	[4]

a Total current density distribution across experimental groups.

b CH_4 partial current density profiles within experimental groups.

References

1 Y. Liu, M. Zhang, K. Bao, H. Huang and Z. Kang, *ChemSusChem*, 2024, DOI: 10.1002/cssc.202401314, e202401314.

2 M. K. Kim, H. J. Kim, H. Lim, Y. Kwon and H. M. Jeong, *Electrochim Acta*, 2019, **306**, 28-34.

3 M. Li, F. Zhang, M. Kuang, Y. Ma, T. Liao, Z. Sun, W. Luo, W. Jiang and J. Yang, *Nano-Micro Lett*, 2023, **15**, 238.

4 P. Yu, X. Lv, Q. Wang, H. Huang, W. Weng, C. Peng, L. Zhang and G. Zheng, *Small*, 2023, **19**, 2205730.